 CMES, vol.4, no.2, pp.287-299, 2003

Finite-Element Nonlinear Dynamics of Flexible Structures in Three Dimensions

S. Okamoto[1] **and Y. Omura**[1]

Abstract: The purpose of this study is to develop a procedure for performing a dynamic analysis in the case that a structure undergoes large translational and rotational displacements when moving along a nonlinear trajectory at variable velocity. Finite-element equations of motion that include the inertial force of the structure's motion have been derived. The equations also account for the geometric nonlinearity that has to be considered in a problem of finite translational and rotational displacements. A finite rotational matrix was used to transfer vectors or matrices measured in a certain coordinate frame to those measured in another coordinate frame. The computational code for simulating body behavior was developed using the derived equations. The validity of the formulations and the computational code was verified by comparing the numerical solutions obtained using the computational code with our experimental results and the analytical solutions of another researcher. As an application of the new method, the time history response of a model system for movement along an arc trajectory was calculated using the developed computational code.

keyword: Finite rotation, large displacement, flexible structure, dynamics, finite element method, time-integration method, air resistance.

1 Introduction

The international space station, currently under construction with international cooperation, is a large and complex structure, and future space structures may be even larger and more complex. These structures are delivered into an orbit around the earth, and may be delivered in regions of space out of the range of the earth in the future. Consequently, the weight of members and parts of space structures must be reduced. Lightened and enlarged structures would become flexible and undergo significant deformation when subjected to a load due to their reduced stiffness. If robot arms become flexible due to such lightening, the consequent deformation will reduce the controllability of position and orientation. A number of studies on large displacements of flexible structures have been conducted to date, however, most are based on statistical methods [Maeda and Hayashi (1976); Goto (1983)], with only a few employing a dynamic analysis [Bathe, Ramm and Wilson (1975); Zui, Inoue, Imura and Fujikawa (1986); Iura and Atluri (1988); Zupan and Saje (2003)]. To the best of our knowledge, there have been no studies involving the dynamic analysis of a flexible structure moving along a nonlinear trajectory at variable velocity.

In the present study, the acceleration of an arbitrary point in a flexible 3D structure moving along a nonlinear trajectory is derived, followed by the derivation of the finite-element equations of motion considering the acceleration. A computational code for time history response analysis of 3D-framed structures is then developed. The performance of the Newmark method and modified Newton method was evaluated in order to select the most effective time-integration method for nonlinear dynamics [Okamoto and Omura (2000)]. Experiments on the static bending and free vibration of cantilevers, and frame motion when a cantilever moves along a nonlinear trajectory, were carried out in order to compare the numerical solutions with the experimental results. By comparing the numerical solutions with our experimental results and the analytical results for the static bending of cantilevers by Holden (1972), the validity of the formulations in regard to the finite rotational matrices, the nonlinear geometric stiffness matrices, and the vector of nodal point forces equivalent to the element stresses, was established [Okamoto and Omura (1998)]. The consideration of not only the viscous damping force due to internal friction of a body but also air resistance is discussed in the case that a body undergoes large displacements at high speed in air, based on a comparison of the experimental and numerical results for free vibration. Finally, as an application of the proposed method, a comparison is made be-

[1] Department of Mechanical System Engineering, Hiroshima University, Kagamiyama, Higashi-Hiroshima, 739-8527 Japan

tween the numerical solutions and the experimental values for when the clamped end of a cantilever moves along an arc trajectory.

2 Formulations

In developing the finite-element equations, we used the updated Lagrangian (UL) formulation. The expressions developed for general motion were such that the coordinate frame fixed to the body, namely the global coordinate frame, is not the inertial frame, and moves along a nonlinear trajectory at variable velocity. We also consider that the body undergoes large translational and rotational displacements, yet strains remain small. This means that the strains in the coordinate frame fixed to the finite element remain infinitesimal, while the same coordinate frame undergoes large translational and rotational displacements.

2.1 Coordinate frames

The schematics of body motion and the coordinate frames are shown in Figs. 1 and 2. In the figures, the $O-X_1X_2X_3$ frame is the inertial coordinate frame that moves with linear uniform velocity, and ${}^*o-{}^*x_1\ {}^*x_2\ {}^*x_3$ and ${}^*o^j-{}^*x_1^j\ {}^*x_2^j\ {}^*x_3^j$ are the global and j-th element frames at time $*(=0,\ t,$ or $t+\Delta t)$, respectively. The $o-x_1x_2x_3$ frame is the global coordinate frame observed in the global frame, that is, $o={}^0o$, ${}^to$ or ${}^{t+\Delta t}o$, and $x_k={}^0x_k$, ${}^tx_k$ or ${}^{t+\Delta t}x_k$ (k=1, 2 or 3).

2.2 Displacement

Let's assume that a body elastically deforms as it undergoes translational and rotational motion. An arbitrary point ${}^0p$ in the body at time 0 moves to the point ${}^tp$ at time t, and then ${}^{t+\Delta t}p$ at time $t+\Delta t$, as shown in Fig. 2. When the total displacements at points ${}^tp$ and ${}^{t+\Delta t}p$, and the incremental displacement during Δt measured in the element coordinate frame at time t are denoted by ${}_{e'}{}^t\boldsymbol{u}$, ${}^{t+\Delta t}_{e'}\boldsymbol{u}$ and ${}_{e'}\Delta\boldsymbol{u}$, total displacements are given by

$$ {}^{t+\Delta t}_{e'}\boldsymbol{u} = {}_{e'}{}^t\boldsymbol{u} + {}_{e'}\Delta\boldsymbol{u} \tag{1} $$

A physical quantity measured in the inertial, the global or the element coordinate frame at time 0, t, or $t+\Delta t$, is appended the symbol i, g, e, i', g', e', i'', g'' or e'' at the lower left. Here, i=i'=i''.

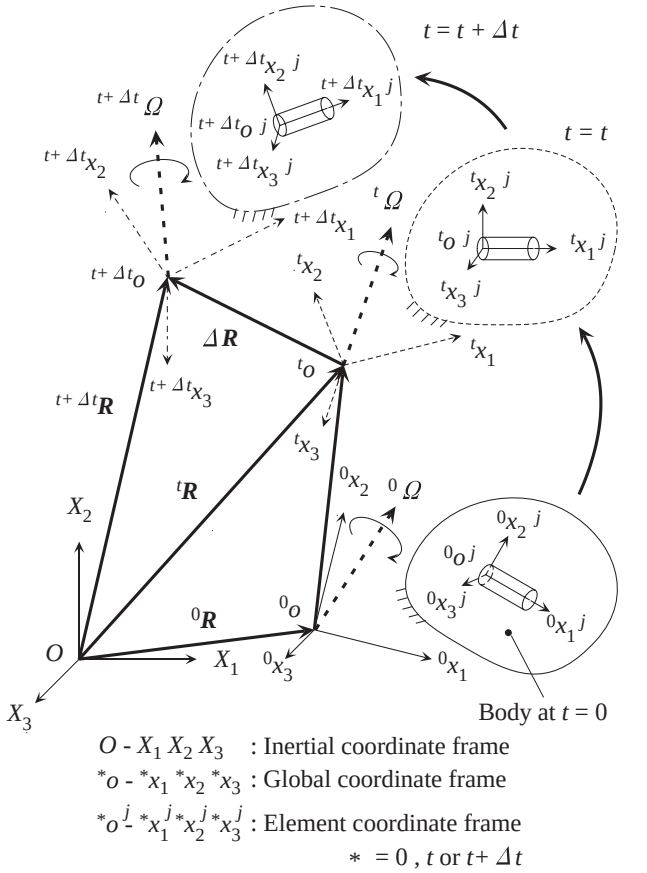

Figure 1 : Body motion in inertial coordinate frame

2.3 Absolute acceleration

The absolute acceleration ${}^{t+\Delta t}_{e'}\boldsymbol{a}$ at the point ${}^{t+\Delta t}p$ measured in the element coordinate frame at time t is given by

$$ \begin{aligned} {}^{t+\Delta t}_{e'}\boldsymbol{a} &= \boldsymbol{T}_{e'i''}\ {}^{t+\Delta t}_{i''}\ddot{\boldsymbol{R}} + \boldsymbol{T}_{e'g''}\{\ {}^{t+\Delta t}_{g''}\ddot{\boldsymbol{r}} \\ &+ {}^{t+\Delta t}_{g''}\dot{\Omega}\times\ {}^{t+\Delta t}_{g''}\boldsymbol{r} + 2\ {}^{t+\Delta t}_{g''}\Omega\times\ {}^{t+\Delta t}_{g''}\dot{\boldsymbol{r}} \\ &+ {}^{t+\Delta t}_{g''}\Omega\times(\ {}^{t+\Delta t}_{g''}\Omega\times\ {}^{t+\Delta t}_{g''}\boldsymbol{r})\} \end{aligned} \tag{2} $$

where ${}^{t+\Delta t}_{i''}\boldsymbol{R}$ is the position vector of the origin ${}^{t+\Delta t}o$ measured in the inertial coordinate frame at time $t+\Delta t$, and ${}^{t+\Delta t}_{g''}\Omega$ is the rotational angular velocity of the body measured in the global coordinate frame at time $t+\Delta t$, as shown in Fig. 1. The matrix $\boldsymbol{T}_{e'i''}$ denotes the transfer matrix of a finite rotation to transfer the vector quantities measured in the inertial coordinate frame at time $t+\Delta t$ to those measured in the element coordinate frame at time t, and $\boldsymbol{T}_{e'g''}$ denotes the transfer matrix of a finite rotation to transfer the vector quantities measured in the global

coordinate frame at time $t+\Delta t$ to those measured in the element coordinate frame at time t, where $\boldsymbol{T}^T_{e'g''}=\boldsymbol{T}_{g''e'}$. The vector ${}^{t+\Delta t}_{g''}\boldsymbol{r}$ denotes the position vector with initial and end points $o\ (={}^{t+\Delta t}o)$ and ${}^{t+\Delta t}p$, respectively, as shown in Fig. 2. Then, ${}^{t+\Delta t}_{g''}\boldsymbol{r}$ is given by the following expression using the position vector ${}_{g'}{}^{t}\boldsymbol{r}$ and the incremental displacement ${}_{e'}\Delta\boldsymbol{u}$:

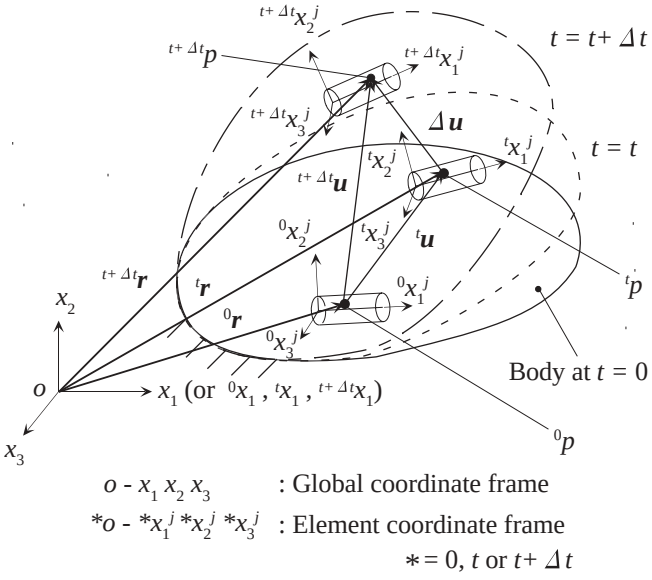

Figure 2 : Body motion in global coordinate frame

$$ {}^{t+\Delta t}_{g''}\boldsymbol{r} = \boldsymbol{T}_{g''g'}\,{}_{g'}{}^{t}\boldsymbol{r} + \boldsymbol{T}_{g''e'}\,{}_{e'}\Delta\boldsymbol{u} \tag{3} $$

where $\boldsymbol{T}_{g''g'}$ denotes the transfer matrix of a finite rotation to transfer the vector quantities measured in the global coordinate frame at time t to those measured in the global coordinate frame at time $t+\Delta t$. Substituting Eq. (3) into Eq. (2) yields the following expression:

$$ \begin{aligned} {}^{t+\Delta t}_{e'}\boldsymbol{a} &= \boldsymbol{T}_{e'i''}\,{}^{t+\Delta t}_{i''}\ddot{\boldsymbol{R}} + \boldsymbol{T}_{e'g'}\,{}_{g'}{}^{t}\ddot{\boldsymbol{r}} \\ &+ \boldsymbol{T}_{e'g''}\{\,{}^{t+\Delta t}_{g''}\dot{\Omega}\times(\boldsymbol{T}_{g''g'}\,{}_{g'}{}^{t}\boldsymbol{r} + \boldsymbol{T}_{g''e'}\,{}_{e'}\Delta\boldsymbol{u})\} \\ &+ 2\boldsymbol{T}_{e'g''}\{\,{}^{t+\Delta t}_{g''}\Omega\times(\boldsymbol{T}_{g''g'}\,{}_{g'}{}^{t}\dot{\boldsymbol{r}} + \boldsymbol{T}_{g''e'}\,{}_{e'}\Delta\dot{\boldsymbol{u}})\} \\ &+ \boldsymbol{T}_{e'g''}[\,{}^{t+\Delta t}_{g''}\Omega\times\{\,{}^{t+\Delta t}_{g''}\Omega\times(\boldsymbol{T}_{g''g'}\,{}_{g'}{}^{t}\boldsymbol{r} \\ &+ \boldsymbol{T}_{g''e'}\,{}_{e'}\Delta\boldsymbol{u})\}] + {}_{e'}\Delta\ddot{\boldsymbol{u}} \end{aligned} \tag{4} $$

where the component in the x_k - direction of ${}^{t+\Delta t}_{e'}\boldsymbol{a}$ is denoted ${}^{t+\Delta t}_{e'}a_k$.

2.4 Principle of virtual work

A body in equilibrium at time $t+\Delta t$ is shown in Figs. 1 and 2. Here, let us consider the element that include the point ${}^{t+\Delta t}p$ of the body. If the volume and the area of the surface of the element at time t are denoted ${}^tV^e$ and ${}^tS^e$, respectively, the principle of virtual work for the element at time $t+\Delta t$ measured in the element coordinate frame at time t is expressed as

$$ \begin{aligned} &- \int_{{}^tV^e}\delta_{e'}\Delta u_k\,{}^t\rho\ {}^{t+\Delta t}_{e'}a_k\,d^tV^e \\ &- \int_{{}^tV^e}\delta_{e'}\Delta\varepsilon_{kl}\ {}^{t+\Delta t}_{e'}s_{kl}\,d^tV^e \\ &+ \int_{{}^tS^e}\delta_{e'}\Delta u_k\ {}^{t+\Delta t}_{e'}f^S_k\,d^tS^e \\ &+ \int_{{}^tV^e}\delta_{e'}\Delta u_k\ {}^{t+\Delta t}_{e'}f^B_k\,d^tV^e = 0 \end{aligned} \tag{5} $$

where

$$ {}_{e'}\Delta\varepsilon_{kl} = {}_{e'}\Delta\varepsilon^L_{kl} + {}_{e'}\Delta\varepsilon^N_{kl} \tag{6} $$

$$ {}_{e'}\Delta\varepsilon^L_{kl} = \frac{1}{2}\left(\frac{\partial_{e'}\Delta u_k}{\partial^t x_l} + \frac{\partial_{e'}\Delta u_l}{\partial^t x_k}\right) \tag{7} $$

$$ {}_{e'}\Delta\varepsilon^N_{kl} = \frac{1}{2}\left(\frac{\partial_{e'}\Delta u_m}{\partial^t x_l}\frac{\partial_{e'}\Delta u_m}{\partial^t x_k}\right) \tag{8} $$

Here, ${}^{t+\Delta t}_{e'}s_{kl}$ is the second Piola-Kirchhoff stress and ${}_{e'}\Delta\varepsilon_{kl}$ is the incremental Green-Lagrange strain. Then, ${}^{t+\Delta t}_{e'}f^S_k$ is the surface force and ${}^{t+\Delta t}_{e'}f^B_k$ is the body force.

2.5 Finite-element equations of motion

The finite-element equation of motion derived from Eq. (5) is expressed as

$$ \begin{aligned} &{}^{t+\Delta t}_{e'}\boldsymbol{f}_a + {}^{t+\Delta t}_{e'}\boldsymbol{f}_v + \left\{{}_{e'}{}^{t}\boldsymbol{f}_\tau + \left({}_{e'}\boldsymbol{K}_e + {}_{e'}{}^{t}\boldsymbol{K}_\tau\right){}_{e'}\Delta\boldsymbol{d} + {}_{e'}\boldsymbol{O}(2)\right\} \\ &\quad = {}^{t+\Delta t}_{e'}\boldsymbol{f}_e \end{aligned} \tag{9} $$

where

$$ {}^{t+\Delta t}_{e'}\boldsymbol{f}_a = \int_{{}^tV^e} {}_{e'}\boldsymbol{N}^T\, {}^t\rho\, {}^{t+\Delta t}_{e'}\boldsymbol{a}\; d^tV^e \tag{10} $$

$$ {}^t_{e'}\boldsymbol{f}_\tau = \int_{{}^tV^e} {}_{e'}\boldsymbol{B}_L{}^T\, {}^t_{e'}\tau\; d^tV^e \tag{11} $$

$$ {}_{e'}\boldsymbol{K}_e = \int_{{}^tV^e} {}_{e'}\boldsymbol{B}_L{}^T\, \boldsymbol{D}\; {}_{e'}\boldsymbol{B}_L\; d^tV^e \tag{12} $$

$$ {}^t_{e'}\boldsymbol{K}_\tau = \int_{{}^tV^e} {}_{e'}\boldsymbol{B}_N{}^T\, {}^t_{e'}\hat{\tau}\; {}_{e'}\boldsymbol{B}_N\; d^tV^e \tag{13} $$

$$ {}^{t+\Delta t}_{e'}\boldsymbol{f}_e = \int_{{}^tV^e} {}_{e'}\boldsymbol{N}^T\, {}^{t+\Delta t}_{e'}\boldsymbol{f}^B\; d^tV^e + \int_{{}^tS^e} {}_{e'}\boldsymbol{N}^T\, {}^{t+\Delta t}_{e'}\boldsymbol{f}^S\; d^tS^e \tag{14} $$

Here, ${}^{t+\Delta t}_{e'}\boldsymbol{f}_a$ is the inertial force in terms of absolute acceleration, ${}^{t+\Delta t}_{e'}\boldsymbol{f}_v$ is the viscous damping force due to internal friction of the element, ${}^t_{e'}\boldsymbol{f}_\tau$ is the vector of nodal point forces equivalent to the element stresses at time t, ${}_{e'}\boldsymbol{O}(2)$ is a second-order term or higher, ${}^{t+\Delta t}_{e'}\boldsymbol{f}_e$ is the external force, ${}_{e'}\boldsymbol{K}_e$ is the linear strain stiffness matrix, ${}^t_{e'}\boldsymbol{K}_\tau$ is the nonlinear geometric stiffness matrix, ${}_{e'}\Delta\boldsymbol{d}$ is the vector of increments in the nodal point displacements, ${}_{e'}\boldsymbol{N}$ is the shape function matrix, ${}_{e'}\boldsymbol{B}_L$ is the linear strain-displacement transformation matrix, ${}_{e'}\boldsymbol{B}_N$ is the nonlinear strain-displacement transformation matrix, $\boldsymbol{D}$ is the elasticity matrix, ${}^t_{e'}\tau$ is the vector of Cauchy stresses, and ${}^t_{e'}\hat{\tau}$ is the matrix of Cauchy stresses. The detail of the derivation of ${}^t_{e'}\boldsymbol{f}_\tau$, ${}_{e'}\boldsymbol{K}_e$ and ${}^t_{e'}\boldsymbol{K}_\tau$ is described in the literatures [Okamoto and Omura (1995); Batha (1996)].

If the viscous damping force ${}^{t+\Delta t}_{e'}\boldsymbol{f}^j_v$ due to internal friction in the element is proportional to the velocity, it is given by

$$ {}^{t+\Delta t}_{e'}\boldsymbol{f}_v = {}^{t+\Delta t}_{e'}\boldsymbol{C}\; {}^{t+\Delta t}_{e'}\dot{\boldsymbol{d}} \tag{15} $$

where ${}^{t+\Delta t}_{e'}\boldsymbol{C}$ is the viscous damping matrix and ${}^{t+\Delta t}_{e'}\dot{\boldsymbol{d}}$ is the vector of nodal point velocities. Further more, if proportional viscous damping can be assumed, the matrix ${}^{t+\Delta t}_{e'}\boldsymbol{C}$ is expressed as

$$ {}^{t+\Delta t}_{e'}\boldsymbol{C} = \alpha\; {}_{e'}\boldsymbol{K}_e \tag{16} $$

where α is a constant.

It is impossible to ignore air resistance when a body undergoes large displacements at high speed in air. Morison's force [JSME (1998)] is used here for air resistance, given by

$$ {}^{t+\Delta t}_{e'}\boldsymbol{f}_m = {}^{t+\Delta t}_{e'}\boldsymbol{f}_{\tilde{v}} + {}^{t+\Delta t}_{e'}\boldsymbol{f}_{\tilde{a}} \tag{17} $$

where ${}^{t+\Delta t}_{e'}\boldsymbol{f}_m$ is Morison's force, ${}^{t+\Delta t}_{e'}\boldsymbol{f}_{\tilde{v}}$ is the drag due to the velocity of air, and ${}^{t+\Delta t}_{e'}\boldsymbol{f}_{\tilde{a}}$ is the inertial resistance due to the acceleration of air. For example, in the case of the two-node element shown in Fig. 3, the drag and inertial resistance are given by

$$ {}^{t+\Delta t}_{e'}f_{\tilde{v}\,i} = C_D\,\frac{\rho_f\,{}^tS_i}{2}\; {}^{t+\Delta t}_{e'}\dot{d}_i\,\left|\,{}^{t+\Delta t}_{e'}\dot{d}_i\right|\;, \quad (i=1\sim3,7\sim9) \tag{18} $$

$$ {}^{t+\Delta t}_{e'}f_{\tilde{a}\,i} = C_m\,\frac{\rho_f\,{}^tV^e}{2}\; {}^{t+\Delta t}_{e'}\ddot{d}_i\;, \quad (i=1\sim3,7\sim9) \tag{19} $$

where ${}^{t+\Delta t}_{e'}f_{\tilde{v}\,i}$ and ${}^{t+\Delta t}_{e'}f_{\tilde{a}\,i}$ are the components of ${}^{t+\Delta t}_{e'}\boldsymbol{f}_{\tilde{v}}$ and ${}^{t+\Delta t}_{e'}\boldsymbol{f}_{\tilde{a}}$, respectively. The components of $i=4\sim6$ and $10\sim12$ are assumed to be zero. In these equations, C_D is the drag coefficient, C_m is the added mass coefficient, ρ_f is the mass density of air, and ${}^tS_k$ is the area of the surface vertical to the x_k - axis.

The equation of motion accounting for both the viscous damping force due to internal friction and air resistance is given by

$$ {}^{t+\Delta t}_{e'}\boldsymbol{f}_{\overline{a}} + {}^{t+\Delta t}_{e'}\boldsymbol{f}_{\overline{v}} + \left\{{}^t_{e'}\boldsymbol{f}_\tau + \left({}_{e'}\boldsymbol{K}_e + {}^t_{e'}\boldsymbol{K}_\tau\right){}_{e'}\Delta\boldsymbol{d} + {}_{e'}\boldsymbol{O}(2)\right\} = {}^{t+\Delta t}_{e'}\boldsymbol{f}_e \tag{20} $$

where

$$ {}^{t+\Delta t}_{e'}\boldsymbol{f}_{\overline{a}} = {}^{t+\Delta t}_{e'}\boldsymbol{f}_a + {}^{t+\Delta t}_{e'}\boldsymbol{f}_{\tilde{a}} \tag{21} $$

$$ {}^{t+\Delta t}_{e'}\boldsymbol{f}_{\overline{v}} = {}^t_{e'}\boldsymbol{C}\; {}^{t+\Delta t}_{e'}\dot{\boldsymbol{d}} + {}^{t+\Delta t}_{e'}\boldsymbol{f}_{\tilde{v}} \tag{22} $$

Hereafter, the symbol j at the upper right of vectors and matrices indicates expressions for the j-th element. If Eq. (20) is transferred to the equation measured in the global coordinate frame at time $t+\Delta t$ using the transfer matrix $\boldsymbol{T}_{g''e'}$, i.e.

$$ {}^{t+\Delta t}_{g''}\boldsymbol{f}^j_{\overline{a}} + {}^{t+\Delta t}_{g''}\boldsymbol{f}^j_{\overline{v}} + \left\{{}^t_{g''}\boldsymbol{f}^j_\tau + \left({}_{g''}\boldsymbol{K}^j_e + {}^t_{g''}\boldsymbol{K}^j_\tau\right){}_{g''}\Delta\boldsymbol{d}^j + {}_{g''}\boldsymbol{O}^j(2)\right\} = {}^{t+\Delta t}_{g''}\boldsymbol{f}^j_e \tag{23} $$

where

$$
\begin{aligned}
{}^{t+\Delta t}_{g''}\boldsymbol{f}^{\,j}_{\overline{a}} &= \boldsymbol{T}^{j}_{g''e'}\ {}^{t+\Delta t}_{e'}\boldsymbol{f}^{\,j}_{\overline{a}} && (24)\\
{}^{t+\Delta t}_{g''}\boldsymbol{f}^{\,j}_{\overline{v}} &= \boldsymbol{T}^{j}_{g''e'}\ {}^{t+\Delta t}_{e'}\boldsymbol{f}^{\,j}_{\overline{v}} && (25)\\
{}^{t}_{g''}\boldsymbol{f}^{\,j}_{\tau} &= \boldsymbol{T}^{j}_{g''e'}\ {}^{t}_{e'}\boldsymbol{f}^{\,j}_{\tau} && (26)\\
{}_{g''}\boldsymbol{K}^{j}_{e} &= \boldsymbol{T}^{j}_{g''e'}\ {}_{e'}\boldsymbol{K}^{j}_{e}\ \boldsymbol{T}^{j\ T}_{g''e'} && (27)\\
{}^{t}_{g''}\boldsymbol{K}^{j}_{\tau} &= \boldsymbol{T}^{j}_{g''e'}\ {}^{t}_{e'}\boldsymbol{K}^{j}_{\tau}\ \boldsymbol{T}^{j\ T}_{g''e'} && (28)\\
{}_{g''}\Delta\boldsymbol{d}^{\,j} &= \boldsymbol{T}^{j}_{g''e'}\ {}_{e'}\Delta\boldsymbol{d}^{\,j} && (29)\\
{}_{g''}\boldsymbol{O}^{j}(2) &= \boldsymbol{T}^{j}_{g''e'}\ {}_{e'}\boldsymbol{O}^{j}(2) && (30)\\
{}^{t+\Delta t}_{g''}\boldsymbol{f}^{\,j}_{e} &= \boldsymbol{T}^{j}_{g''e'}\ {}^{t+\Delta t}_{e'}\boldsymbol{f}^{\,j}_{e} && (31)
\end{aligned}
$$

and if the equations of motion for all elements are generated, namely Eq. (23), then composing all the equations and taking account of boundary conditions gives the equation of motion for the whole body, expressed as

$$
\begin{aligned}
&{}^{t+\Delta t}_{g''}\overline{\boldsymbol{f}}_{\overline{a}} + {}^{t+\Delta t}_{g''}\overline{\boldsymbol{f}}_{\overline{v}}\\
&\quad + \left\{ {}^{t}_{g''}\overline{\boldsymbol{f}}_{\tau} + \left({}_{g''}\overline{\boldsymbol{K}}_{e} + {}^{t}_{g''}\overline{\boldsymbol{K}}_{\tau} \right) {}_{g''}\Delta\overline{\boldsymbol{d}} + {}_{g''}\overline{\boldsymbol{O}}(2) \right\}\\
&\quad = {}^{t+\Delta t}_{g''}\overline{\boldsymbol{f}}_{e} \qquad (32)
\end{aligned}
$$

The term of second order or higher ${}_{g''}\overline{\boldsymbol{O}}(2)$ was ignored in the simulations because it is negligibly small relative to the other terms.

2.6 Method of calculation

The computational code for time history response analysis of framed structures in 3D space was developed using the above formulations. Two methods were used to solve Eq. (32), as outlined in the following.

One of the methods used was the Newmark method, which is an extension of the linear acceleration method. The solutions at time $t+\Delta t$ are calculated as if the coefficient matrices of Eq. (32), such as the stiffness matrices were constant from time t to $t+\Delta t$.

The other method used was the modified Newton method, which is an iteration scheme. Below is the formulation for the modified Newton method based on Eq. (32) [see Bathe, Ramm and Wilson (1975)].

$$
\begin{aligned}
&\left({}_{g''}\overline{\boldsymbol{K}}_{e} + {}^{t}_{g''}\overline{\boldsymbol{K}}_{\tau} \right) \Delta \left({}_{g''}\Delta\overline{\boldsymbol{d}} \right)^{(k)} =\\
&{}^{t+\Delta t}_{g''}\overline{\boldsymbol{f}}_{e} - {}^{t+\Delta t}_{g''}\overline{\boldsymbol{f}}^{\,(k)}_{\overline{a}} - {}^{t+\Delta t}_{g''}\overline{\boldsymbol{f}}^{\,(k)}_{\overline{v}} - {}^{t+\Delta t}_{g''}\overline{\boldsymbol{f}}^{\,(k-1)}_{\tau} \qquad (33)
\end{aligned}
$$

$$
\begin{aligned}
{}_{g''}\Delta\overline{\boldsymbol{d}}^{\,(k)} &= {}_{g''}\Delta\overline{\boldsymbol{d}}^{\,(k-1)} + \Delta\left({}_{g''}\Delta\overline{\boldsymbol{d}} \right)^{(k)} && (34)\\
{}_{g''}\Delta\ddot{\overline{\boldsymbol{d}}}^{\,(k)} &= \frac{1}{\beta\,(\Delta t)^2}\,{}_{g''}\Delta\overline{\boldsymbol{d}}^{\,(k)} - \frac{1}{\beta\,\Delta t}\,{}^{t}_{g''}\dot{\overline{\boldsymbol{d}}} - \frac{1}{2\,\beta}\,{}^{t}_{g''}\ddot{\overline{\boldsymbol{d}}} && (35)\\
{}_{g''}\Delta\dot{\overline{\boldsymbol{d}}}^{\,(k)} &= \Delta t\,(1-\gamma)\,{}^{t}_{g''}\ddot{\overline{\boldsymbol{d}}} - \Delta t\,\gamma\ {}^{t+\Delta t}_{g''}\ddot{\overline{\boldsymbol{d}}}^{\,(k)} && (36)
\end{aligned}
$$

where β and γ are parameters that determine integration accuracy and stability. The superscripts $(k-1)$ and (k) refer to the number of iterations. The calculations are iterated until the appropriate convergence criteria are satisfied. The modified Newton method corresponds to the condition that acceleration from time t to $t+\Delta t$ can be interpolated by a curved line.

3 Experiments

Experiments were conducted for a cantilever under three conditions: static bending, free vibration and frame motion when the clamped end of the cantilever moves along a nonlinear trajectory.

3.1 Static bending

A brass cantilever of length $0.9\,[m]$ and diameter $3\,[mm]$ was used in the static bending experiment. The displacement of the cantilever due to a tare load alone was measured, followed by measurements of both a tare load on the cantilever and a concentrated load on the free end due to a weight of 50, 100 or $150\,[g]$. The weight was limited to $150\,[g]$ so as not to exceed the elastic limit of the cantilever. The physical parameters of brass are listed in Table 1.

3.2 Free vibration

A stainless steel cantilever was used in the free vibration experiment. The length of the cantilever was $0.9\,[m]$, and the width and height of the rectangular cross-section were $6\,[mm]$ and $2\,[mm]$, respectively. The physical parameters of stainless steel are listed in Table 1.

Method of measurement The vibration of the cantilever was captured by video camera. Time history response data were generated from the video by processing on a personal computer.

3.3 Frame motion

An experiment on frame motion in the case that the clamped end of a cantilever moves along a nonlinear trajectory was carried out. An aluminum cantilever

was used in this experiment, with dimensions $1.0\,[m] \times 20\,[mm] \times 2\,[mm]$. The physical parameters of aluminum are listed in Table 1. The behavior of the body was captured by the same method as that used in the free vibration experiment.

4 Results

4.1 Analysis model

In the simulations, analysis models idealizing the cantilevers used in the experiments were used. The analysis models were divided into two-node elements, as shown in Fig. 3.

4.2 Static bending

The analysis model used in the static bending experiment was an idealized cantilever divided into nine two-node elements.

Table 1 : Physical parameters

	Brass	Stainless steel	Aluminum
ρ	8.53×10^3	8.03×10^3	2.71×10^3
E	110×10^9	197×10^9	69×10^9
ν	0.33	0.34	0.28

ρ : Mass density $\left[kg/m^3\right]$
E : Young's modulus $\left[N/m^2\right]$
ν : Poisson's ratio

The Newmark method ($\beta = 1/4$) was used for time integration. Initially, the displacement due to a tare load alone was calculated. In the simulation, the tare load on the cantilever was gradually increased quasi-statically up to a level equal to gravitational acceleration ($g = 9.8\,[m/s^2]$). Then the displacements due to both a tare load on the cantilever and a concentrated load on the free end were calculated such that the system became quasi-static. The numerical solutions and experimental values are shown in Fig. 4.

The displacement of the free end of the cantilever under a uniformly distributed load was calculated. The results are shown in Fig. 5, in which the solid line is the numerical solution obtained in this study and the dot-dash line is the analytical solution by Holden (1972); the two solutions are in good agreement.

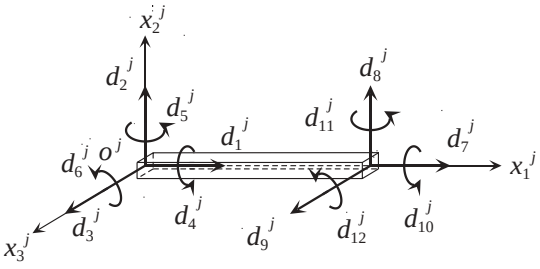

Figure 3 : Two-node element

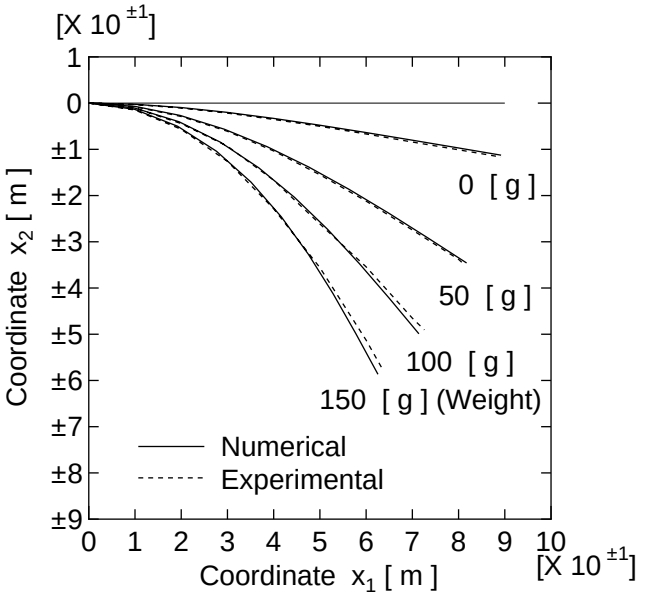

Figure 4 : Deformation of cantilever under both tare load and concentrated load on free end due to weight

It is clear from these results that the formulations concerning the transfer matrices of finite rotation, the nonlinear geometric stiffness matrices, and the vector of nodal forces equivalent to the element stresses, are all relevant.

4.3 Free vibration

The analysis model for the free vibration experiment was divided into nine two-node elements.

The time history response of the cantilever when the free end was loaded with a half-sine-wave force, as shown in Fig. 6, was calculated using the Newmark method ($\beta =$

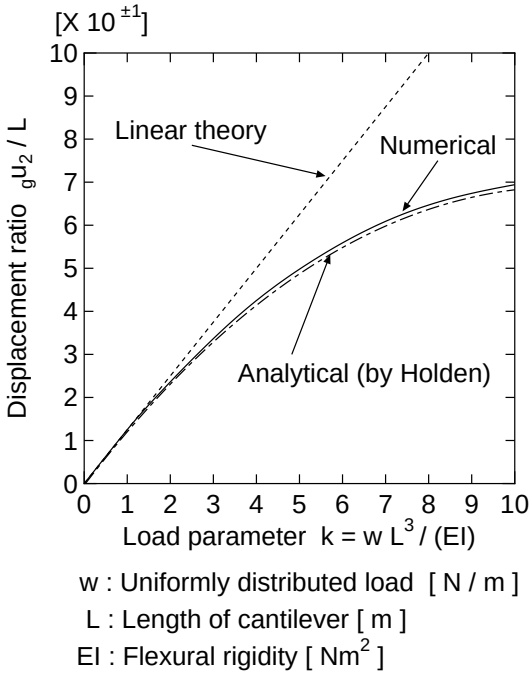

Figure 5 : Displacement of free end of cantilever under uniformly distributed load

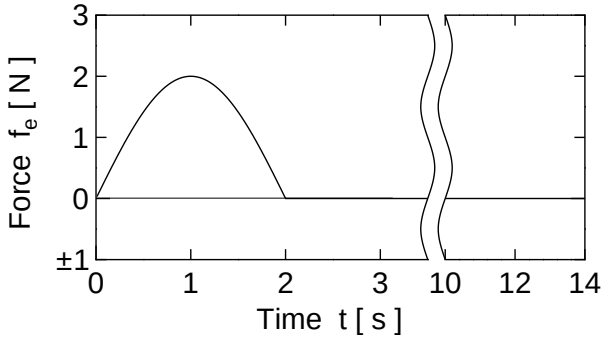

Figure 6 : Half-sine-wave force

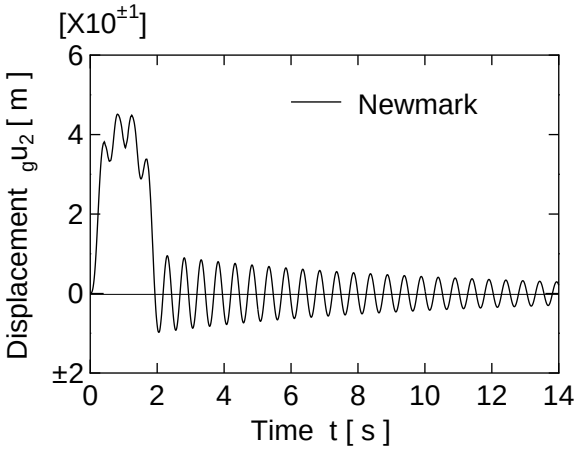

Figure 7 : Lateral displacement of free end of cantilever under half-sine-wave force

$1/4$). The time increment Δt was set at $1.0 \times 10^{-2}\,[s]$ in order to describe the vibrations up to the third mode of bending ($f_3 = 12.4\,[Hz]$). A value of 1.6×10^{-3} was used for the constant of proportional viscous damping α such that the damping ratio ζ was 0.4 %, as found from the experimental results. The numerical solution for the lateral displacement of the free end in the global coordinate frame, the origin of which is fixed to the clamped end of the cantilever, is shown in Fig. 7. The response in the range from $0\,[s]$ to $2\,[s]$ comprises both the free vibration and the forced vibration due to the half-sine-wave force. The response after $2\,[s]$ therefore represents only free vibration.

To examine the effect of applying the force more rapidly, the response of the body to the application of the impulse force shown in Fig. 8 was calculated. The time increment Δt and constant of proportional viscous damping α were the same as for the previous calculation. The numerical solutions for lateral displacement of the free end by the Newmark method ($\beta = 1/4$) and the modified Newton method ($\beta = 1/4$, $\gamma = 1/2$) are shown in Fig. 9. The displacement after application of an impulse force should approach zero, however as can be seen from Fig. 9, the solution by the Newmark method converges to a value greater than zero. This is due to the fact that the modified Newton method has negligible cumulative numerical error because it is based on the condition that the acceleration during Δt is interpolated by a curved line, whereas the Newmark method cumulates a significant numerical error because the acceleration during Δt is interpolated linearly. These results show that the modified Newton method is more effective for dynamic analyses in cases where the acceleration changes rapidly.

4.4 Damping forces

The damping forces were examined by comparing the numerical solutions by the modified Newton method with the experimental values.

The constant of proportional viscous damping α obtained in experiments was $\alpha = 1.6 \times 10^{-3}$ ($\zeta = 0.4\,\%$),

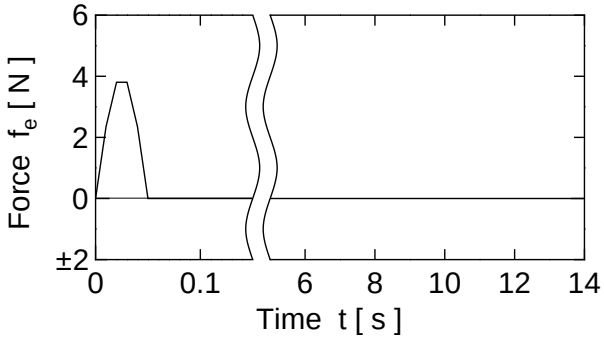

Figure 8 : Impulse force

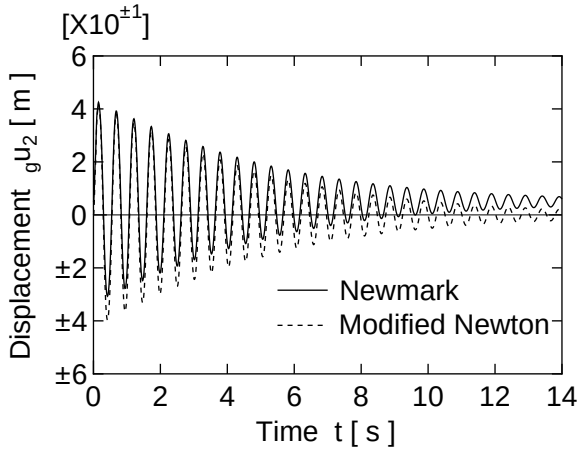

Figure 9 : Lateral displacement of free end of cantilever under impulse force

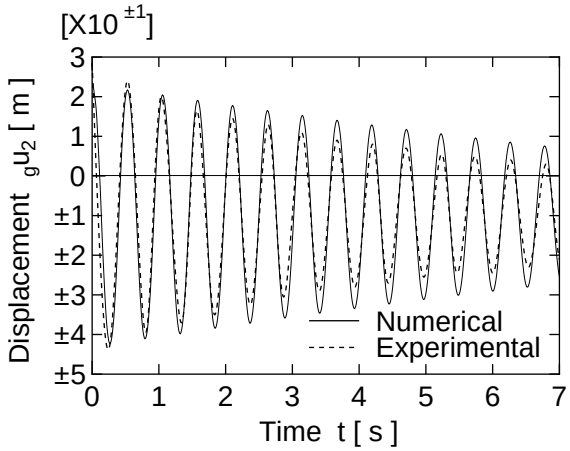

(a) 0 [*s*] to 7 [*s*]

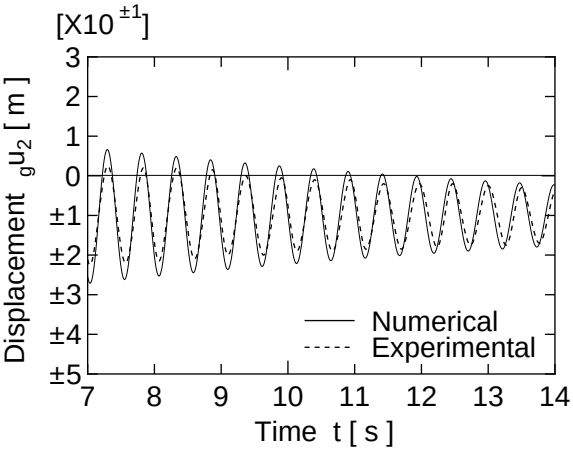

(b) 7 [*s*] to 14 [*s*]

Figure 10 : Lateral displacement of free end of cantilever considering viscous damping force due to internal friction of $\alpha = 1.6 \times 10^{-3}$

found under conditions of free vibration with small displacement. The numerical solutions using this value of $\alpha = 1.6 \times 10^{-3}$ are shown together with the experimental results in Fig. 10. The numerical solution does not match the experimental values when both displacement and velocity are large because α is too small. Numerical solutions using a larger value of α, for example 2.1×10^{-3} ($\zeta = 1.5\,\%$) are shown with the experimental values in Fig. 11. In this case, the numerical solution fits the experimental results when both displacement and velocity are large, yet does not agree well when the displacements are small due to the large α. These results indicate that it is inadequate to consider only the viscous damping force due to internal friction when both displacement and velocity are large.

The behavior of the cantilever considering the viscous damping force due to internal friction and air resistance was also calculated. The constant of proportional viscous damping α was set at 1.6×10^{-3} ($\zeta = 0.4\,\%$), as in the previous experiments. A value of 1.0 was used for the added mass coefficient C_m because the beam is quite long compared with the lengths of the sides of the rectangular cross-section. The drag coefficient C_D due to air resistance was set at 5.0 so as to correspond with the experimental conditions. According to JSME (1998), the drag coefficient C_D for a beam with rectangular cross-section is around 2 when the Reynold's number (*Re*) for the air at relative velocity is between 10^3 and 5×10^3, increasing to 20 to 40 when *Re* is below 10^3. As *Re* in the present simulation is in the range 0 to 1.5×10^3, the C_D of

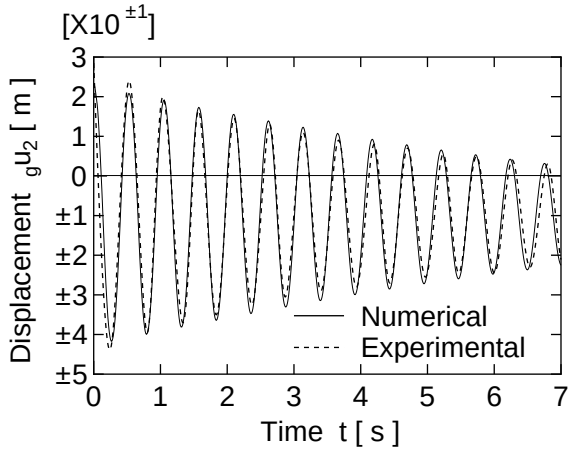

(a) 0 $[s]$ to 7 $[s]$

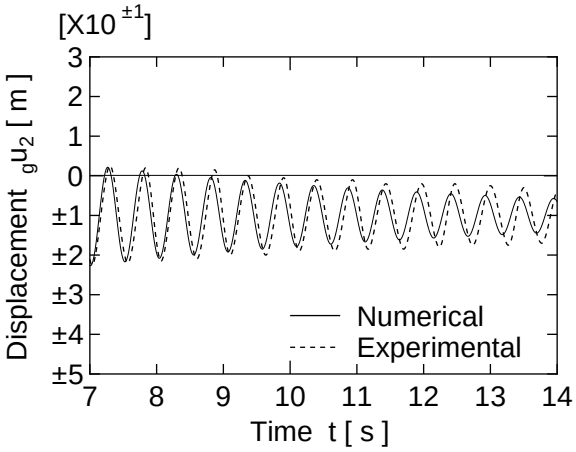

(b) 7 $[s]$ to 14 $[s]$

Figure 11 : Lateral displacement of free end of cantilever considering viscous damping force due to internal friction of $\alpha = 2.1 \times 10^{-3}$

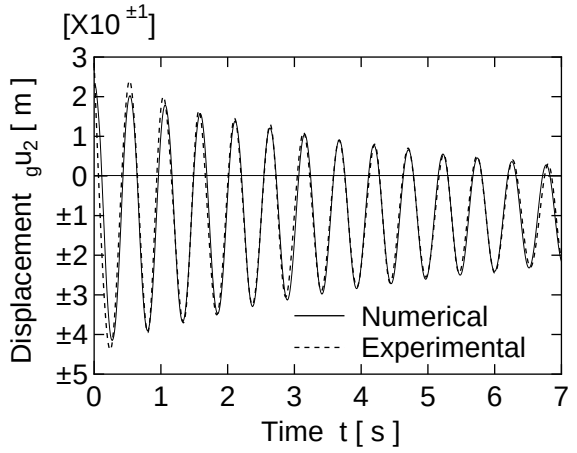

(a) 0 $[s]$ to 7 $[s]$

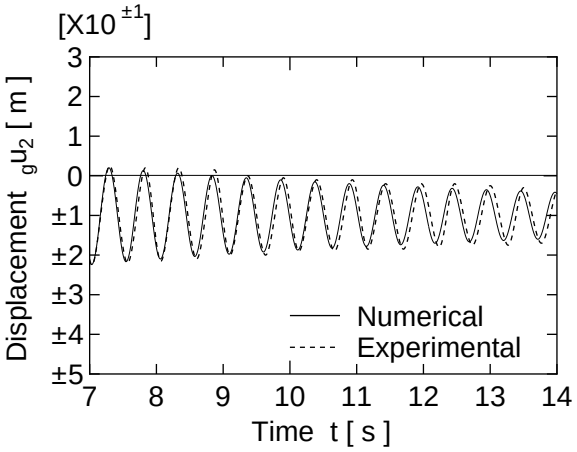

(b) 7 $[s]$ to 14 $[s]$

$\alpha = 1.6 \times 10^{-3}$, $C_m = 1.0$, $C_D = 5.0$

Figure 12 : Lateral displacement of free end of cantilever considering both viscous damping force due to internal friction and air resistance

5.0 used in the simulation is qualitatively accurate. The numerical solution and experimental results are shown in Fig. 12; the close correspondence indicates that considering both viscous damping force due to internal friction and air resistance provides a more accurate solution when displacement and velocity become large.

4.5 Frame motion in two dimensions

The experiment on frame motion was performed by translating the clamped end of a cantilever along an arc trajectory of radius and subtending angle 450 $[mm]$ and $\pi/2$ $[rad]$, respectively. A stop of every stiffness constant of the X_1 -, X_2 - and X_3 - directions 5×10^2 $[N/m]$ $(= k_{s1} = k_{s2} = k_{s3})$ was set the end of the trajectory. The experimental results for each 0.1 $[s]$ are indicated by the broken line in Fig. 13. The time history of displacement in the X_1 - and X_2 - directions, and angle of rotation around the x_3- axis, namely $\Psi_3 = \int_0^t \Omega_3 dt$, of the clamped end in the inertial coordinate frame, the origin of which is the center of the arc, is shown in Figs. 14, 15 and 16, respectively. The time history of displacement of the free end in the X_1 - and X_2 - directions in the inertial coordinate frame is also shown as a broken line in Figs. 17 and 18, respectively.

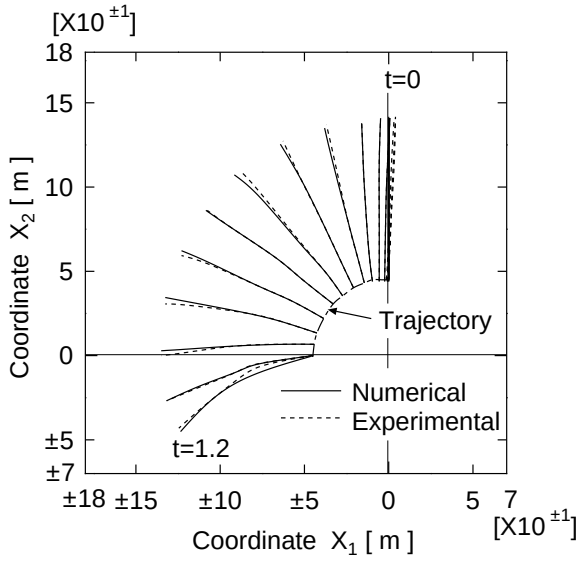

Figure 13 : Frame motion in two dimensions

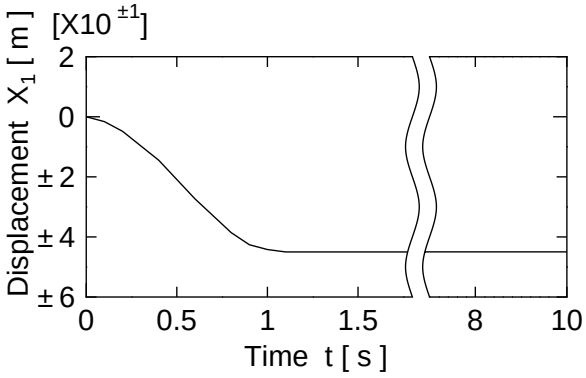

Figure 14 : Displacement of clamped end of cantilever in X_1 - direction

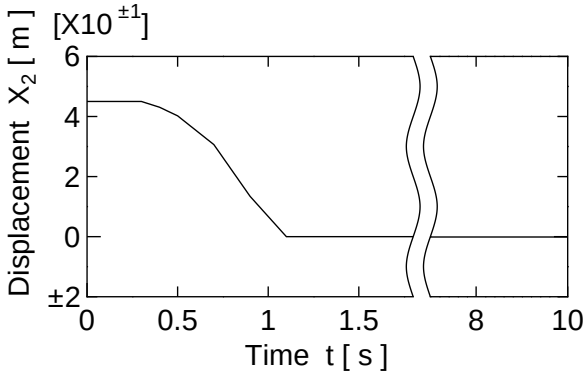

Figure 15 : Displacement of clamped end of cantilever in X_2 - direction

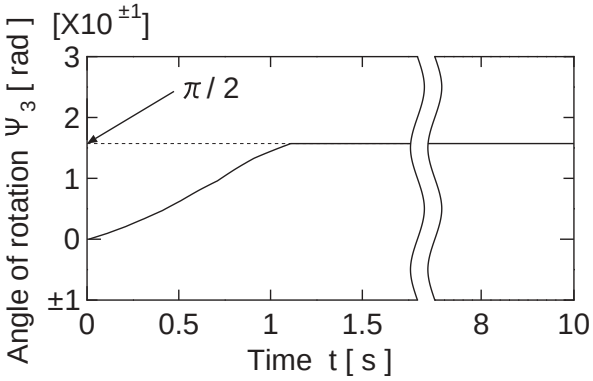

Figure 16 : Angle of rotation of global coordinate frame around x_3 - axis

A simulation reproducing the conditions of the experiment was then carried out. The analysis model was divided into ten two-node elements. The modified Newton method was used as the time-integration scheme. A time increment Δt of $1.0 \times 10^{-2}\,[s]$ was used in order to describe the vibrations up to the third mode of bending ($f_3 = 10.22\,[Hz]$). The constant of proportional viscous damping α was set at 2.0×10^{-3} ($\zeta = 0.9\,\%$), found under conditions of free vibration with small displacement. A drag coefficient C_D and added mass coefficient C_m of 5.0 and 1.0, respectively, were used, consistent with the previous experiments. The numerical solution for each $0.1\,[s]$ is shown as a solid line in Fig. 13. The displacement of the free end in the x_1 - and x_2 - directions is shown as a solid line in Figs. 17 and 18, respectively. The numerical solution is in good agreement with the experimental results.

4.6 Frame motion in three dimensions

A simulation on a three dimensional problem was carried out by translating the clamped end of the cantilever of length and diameter $1.0[m]$ and $4[mm]$, respectively, as well as moving along the arc trajectory in the X_1 - X_2 plane under the same conditions as the two dimensional problem. The same stop as the two dimensional problem was set the end of the trajectory. The time history of displacement of the clamped end in X_3 - direction in the inertial coordinate frame is shown in Fig. 19. By referring to JSME(1998), the drag coefficient C_D and the added mass coefficient C_m for a beam with the circular cross-section were set at 1.0 and 1.0, respectively. The

time increment Δt and the constant of proportional viscous damping α were set at the same values as the two dimensional problem. The numerical solution for each $0.1\,[s]$ is shown in Fig. 20. The displacement of the free end in the X_1 -, X_2 - and X_3 - directions is shown in Figs. 21, 22 and 23, respectively.

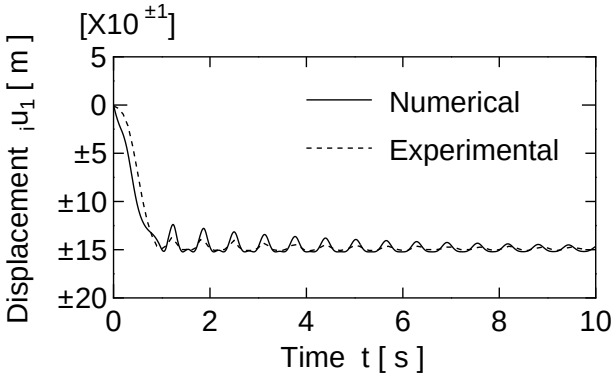

Figure 17 : Displacement of free end of cantilever in X_1 - direction under frame motion in two dimensions

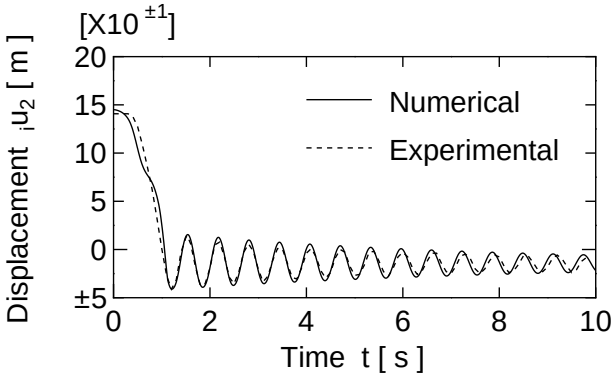

Figure 18 : Displacement of free end of cantilever in X_2 - direction under frame motion in two dimensions

5 Conclusions

The objective of this research was to develop a procedure for performing a dynamic analysis in the case that a flexible structure undergoes large translational and rotational displacements in three dimensions as it moves along a nonlinear trajectory at variable velocity. The finite-element equations of motion considering the inertial force generated when a structure moves along a non-

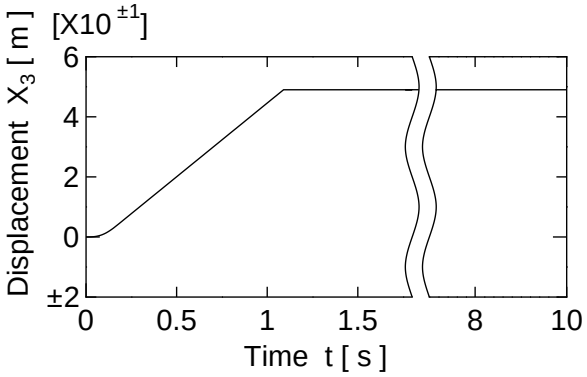

Figure 19 : Displacement of clamped end of cantilever in X_3 - direction under frame motion in three dimensions

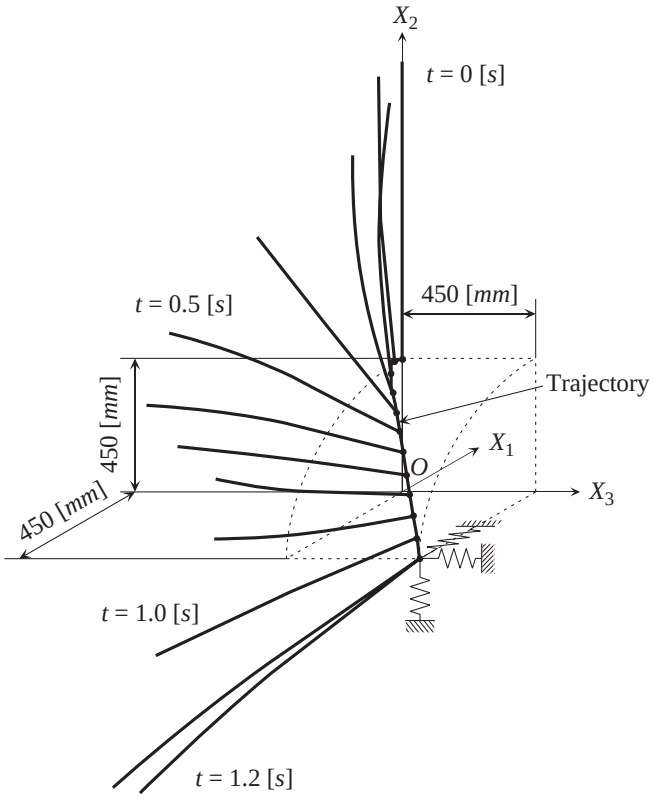

Figure 20 : Frame motion in three dimensions

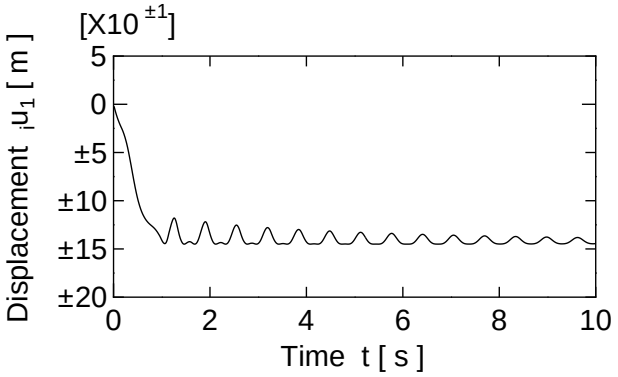

Figure 21 : Displacement of free end of cantilever in X_1 - direction under frame motion in three dimensions

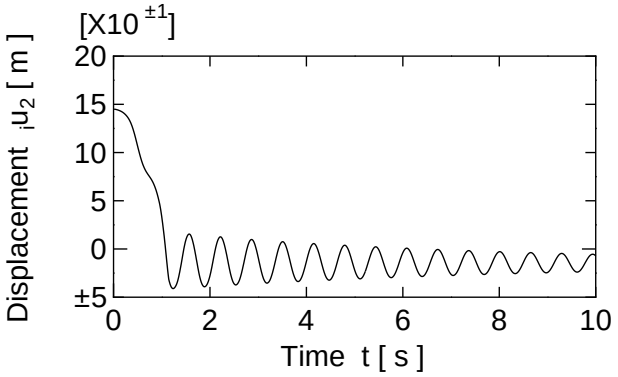

Figure 22 : Displacement of free end of cantilever in X_2 - direction under frame motion in three dimensions

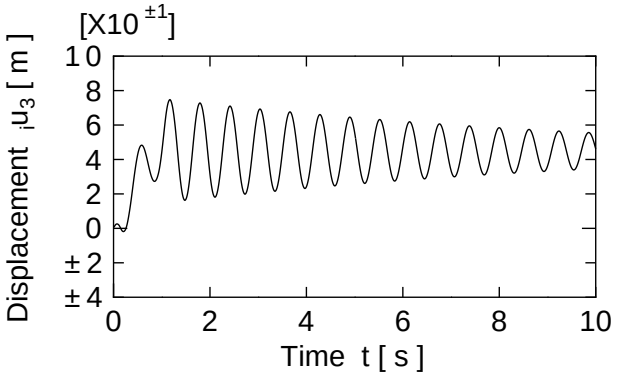

Figure 23 : Displacement of free end of cantilever in X_3 - direction under frame motion in three dimensions

linear trajectory in three dimensions were derived. Furthermore, a computational code for simulating the behavior of a body was developed using the derived equations. The validity of the formulations and the computational code was verified by comparing numerical solutions obtained using the computational code with experimental results and the analytical solutions of another researcher. The results presented in this paper indicated that;

(1) An iteration method such as the modified Newton method is more effective than a linear acceleration method such as the Newmark method as a time-integration scheme for problems in the case that a structure undergoes large translational and rotational displacements with rapid acceleration changes.

(2) Both the viscous damping force due to internal friction of a body and air resistance must be considered when the body undergoes large displacements at high speed in air.

Appendix: Finite rotational matrix

Let the right-handed rotation of the coordinate frame $o-x_1x_2x_3$ around the axial vector $\boldsymbol{\theta}\,(=\theta_1\boldsymbol{e}_1+\theta_2\boldsymbol{e}_2+\theta_3\boldsymbol{e}_3)$ by the finite angle $\theta\,(=|\boldsymbol{\theta}|)$ result in $o-x_1'x_2'x_3'$. In this case, the transfer matrix of a finite rotation $\boldsymbol{T}$ for the transfer of vectors and matrices in $o-x_1x_2x_3$ into a $o-x_1'x_2'x_3'$ frame is given by

$$\boldsymbol{T}=\begin{bmatrix} {\phi_1}^2(1-\cos\theta)+\cos\theta & \phi_1\phi_2(1-\cos\theta)+\phi_3\sin\theta & \phi_3\phi_1(1-\cos\theta)-\phi_2\sin\theta \\ \phi_1\phi_2(1-\cos\theta)-\phi_3\sin\theta & {\phi_2}^2(1-\cos\theta)+\cos\theta & \phi_2\phi_3(1-\cos\theta)+\phi_1\sin\theta \\ \phi_3\phi_1(1-\cos\theta)+\phi_2\sin\theta & \phi_2\phi_3(1-\cos\theta)-\phi_1\sin\theta & {\phi_3}^2(1-\cos\theta)+\cos\theta \end{bmatrix} \tag{37}$$

where ϕ_1, ϕ_2 and ϕ_3 denote the direction cosines of $\boldsymbol{\theta}$, expressed as

$$\phi_1=\frac{\theta_1}{\theta},\quad \phi_2=\frac{\theta_2}{\theta},\quad \phi_3=\frac{\theta_3}{\theta} \tag{38}$$

Batha, K.J. (1996): Finite Element Procedures, *Prentice-Hall, Inc.*, pp.555-557.

Bathe, K. L.; Ramm, E.; Wilson, E. L. (1975): Finite Element Formulations for Large Deformation Dynamic Analysis. *International Journal for Numerical Methods in Engineering*, vol. 9, pp. 353-386.

Goto, S. (1983): A Formulation of Tangent Geometric Stiffness Matrix for Space Structure [in Japanese]. *Transactions of the Japan Society of Civil Engineers*, No. 335, pp. 1-11.

Holden, J. T. (1972): On the Finite Deflections of Thin Beams. *International Journal for Solids Structures*, vol. 8, pp. 1051-1055.

Iura, M.; Atluri, S.N. (1988): Dynamic Analysis of Finitely Stretched and Rotated Three-Dimensional Space-Curved Beam. *Computers and Structures*, vol.29, No.5, pp.875-889.

JSME (Japan Society of Mechanical Engineers) (1998): JSME Standard, Guideline for Evaluation of Flow-Induced Vibration of a Cylindrical Structure in a Pipe [in Japanese]. *Maruzen Corp.*, pp. B6-B20.

Maeda, Y. ; Hayashi, M. (1976): Finite Displacement Analysis of Space Framed Structures [in Japanese]. *Transactions of the Japan Society of Civil Engineers*, No. 253, pp. 13-27.

Okamoto, S.; Omura, Y. (1995): Dynamic Finite Element Analysis of a Geometric Nonlinear Structure Moving along an Arbitrary Trajectory. *Trans. of the Japan Society of Mechanical Engineers*, vol.65, No.638, pp.3883-3889.

Okamoto, S. ; Omura Y. (1998): Dynamic Finite Element Analysis of a Flexible-Framed Structure Moving along an Arbitrary Trajectory. *Modeling and Simulation Based Engineering*, vol. 1, pp. 752-757.

Okamoto, S. ; Omura Y. (2000): Finite Element Dynamics on a Large Deformation Problem of Multibody Systems. *Advances in Computational Engineering and Sciences*, vol. 1, pp. 806-811.

Zui, H.; Inoue, Y.; Imura, A.; Fujikawa, T. (1986): A Study on the Simulation of Link Mechanics (1st Report, Analysis of the Dynamic Responses, Including Elastic Vibration) [in Japanese]. *Transactions of the Japan Society of Mechanical Engineers*, vol. 52, No. 483, pp. 2814-2821.

Zupan, D.; Saje, M. (2003): A New Finite Element Formulation of Three-Dimensional Beam Theory Based on Interpolation of Curvature. *CMES: Computer Modeling in Engineering & Sciences*, vol. 4, No. 2.